Fabrication of Electrochemically Reduced Graphene Oxide Films on Glassy Carbon Electrode by Self-Assembly Method and Their Electrocatalytic Application

ARTICLE *in* THE JOURNAL OF PHYSICAL CHEMISTRY C · FEBRUARY 2013

Impact Factor: 4.77

1 AUTHOR:

S. ABRAHAM JOHN

Gandhigram Rural Institute

120 PUBLICATIONS **1,720** CITATIONS

SEE PROFILE

THE JOURNAL OF PHYSICAL CHEMISTRY C

Article

pubs.acs.org/JPCC

Fabrication of Electrochemically Reduced Graphene Oxide Films on Glassy Carbon Electrode by Self-Assembly Method and Their Electrocatalytic Application

M. Amal Raj and S. Abraham John*

Centre for Nanoscience and Nanotechnology, Department of Chemistry, Gandhigram Rural Institute, Gandhigram 624 302, Dindigul, Tamilnadu, India

Supporting Information

ABSTRACT: We report a simple, facile, and reproducible method for the fabrication of electrochemically reduced graphene oxide (ERGO) films on glassy carbon electrode (GCE) by the self-assembly method. The graphene precursor, graphene oxide (GO), was self-assembled on GCE through a diamine linker which was preassembled on GCE by electrostatic interaction between the positively charged amine and the negatively charged layers of graphene oxide (GO). The oxygen functional groups present on the surface of GO were electrochemically reduced to retain the aromatic backbone of graphene. The attachment of GO followed by its electrochemical reduction was confirmed by ATR-FT-IR spectroscopy, Raman spectroscopy, X-ray diffraction (XRD), X-ray photoelectron spectroscopy (XPS), atomic force microscopy (AFM), and scanning electron microscopy (SEM). Raman spectra show that the intensity ratio of D and G bands was increased after the electrochemical reduction of GO. XPS results reveal that the carbon-to-oxygen ratio was increased after the electrochemical reduction of electrostatically assembled GO. Further, Raman and XPS results confirm the removal of oxygen functional groups present on the surface of GO after electrochemical reduction. Impedance spectral studies show that the electron transfer reaction was facile at ERGO modified GCE. Finally, the electrocatalytic activity of ERGO was examined by studying the oxidations of ascorbic acid (AA), dopamine (DA), and uric acid (UA). It enhanced the oxidation currents of AA, DA, and UA when compared to bare GCE. The electrocatalytic activity of the present modified electrode was highly stable.

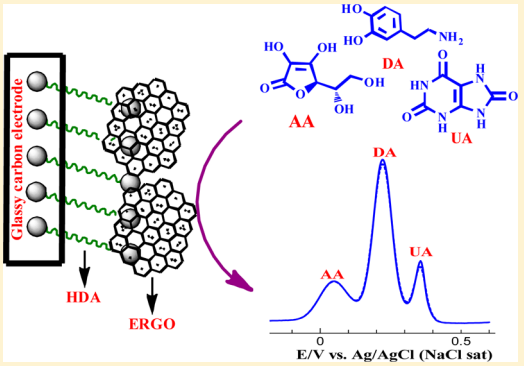

INTRODUCTION

Graphene, the mother of all graphitic materials, comprises a single layer of carbon atoms joined together by sp^2 covalent bonds.[1,2] It is described as an individual of graphite which is made of many graphite layers held together by van der Waals force of attraction.[1,3] The most interesting properties of graphene including high mechanical strength,[4] tunable optical properties,[5] quantum Hall effect,[6] high electron mobility,[7] and fast heterogeneous electron transfer rate[8] make them to be used in variety of fields such as nanoelectronics,[9,10] supercapacitors,[11] batteries,[12] sensors,[13,14] and fuel cells.[15,16] Graphene exfoliation can be achieved by thermal expansion, chemical modification, intercalation, oxidation and reduction, and a combination of any of these methods.[17−23] Among the various methods, oxidation of graphite by strong oxidizing agents to form graphene oxide (GO), a nonconductive hydrophilic carbon material, received great attention due to its easy synthetic protocol. The introduction of functional groups like epoxide, alcohols, ketone, and carboxylic acid by the disruption of aromatic lattice makes GO to be hydrophilic in nature.[24] Staudenmaier and Hummer's methods were commonly used for the oxidation of graphite.[25,26] To retain the aromatic backbone, the GO was reduced by different reagents including hydrazine hydrate,[27] hydroquinone,[28] vitamin C,[29] pyrogallol, hot strong alkaline solutions,[30] and hydroxylamine.[31] The GO can also be reduced electrochemically by applying more negative potential which reduce the oxygen functional groups present on the surface of GO.[18,32−35] The electrochemically prepared graphene sheets will be more conducting than that prepared from chemical reduction, and the O/C ratio of electrochemically reduced GO (ERGO) was less than that of chemical methods.[36,37]

Because of its large surface area and high conducting nature, graphene can be used as a suitable material for the fabrication of electrode surface to improve the electrocatalysis.[13] The surface coverage, orientation, and possible interaction from the exposed areas of the underlying electrode are the major challenges in understanding the electrochemistry of graphene.[38−40] Electrochemical reduction of GO has received much greater attention in recent years since it is considered as a green approach in addition a thin film of graphene can be prepared by this method on conducting substrates.[18,33,34,37] For the fabrication of thin films of graphene on conducting substrates, direct electrochemical deposition of GO,[33,34] drop-

Received: January 3, 2013
Revised: February 6, 2013
Published: February 7, 2013

   dx.doi.org/10.1021/jp400066z | J. Phys. Chem. C 2013, 117, 4326−4335

casting of graphene,[41,42] drop-casting of GO followed by its electrochemical reduction,[18,37] spray-coating,[43] spin-coating,[44] and layer-by-layer assembly[45] were mostly used. The thickness and uniformity of graphene films on conducting substrates cannot be controlled by these methods.

The self-assembly method is one of the elegant methods for the fabrication of nanomaterials on conducting substrates.[46,47] Only few reports were available in the literature for the fabrication of graphene on substrates using the self-assembly method.[32,48−53] Shao et al. reported the fabrication and characterization of graphene/*n*-octadecylmercaptan-modified Au electrode via strong hydrophobic interaction between the self-assembled monolayer (SAM) of mercaptan and graphene nanosheets.[48,49] Ramesha and Sampath reported the self-assembly of GO on Au substrate through cystamine SAM by electrostatic interaction.[50] Viinikanoja et al. reported the in-situ spectroelectrochemical characterization of GO on Au electrode attached through mercaptoethylamine linker.[51] Zhang et al. reported the modification of glassy carbon electrode (GCE) with graphene using the SAM of 3-aminopropyltriethoxysilane on activated GCE followed by the self-assembly of GO and its electrochemical reduction.[32,52] Kim et al. reported the self-assembly of GO using amine-terminated grafted surface of ITO followed by the electrochemical reduction of GO for the immobilization of horseradish peroxidase.[53]

Although the above strategies have been successfully used for the preparation of graphene films by electrochemical method, they have several limitations. For example, in the case of aminothiol linkers (cystamine and mercaptoethylamine), the thiol groups attached on Au surface may be desorbed at more negative potential where the reduction of GO occurs. Hence, it is difficult to control the reduction of GO on Au electrode. Further, it has limited potential window and cannot be used for electrocatalytic applications at either more positive potential or negative potential due to the possible cleavage of the Au−S bond. In this paper, we wish to report a simple and facile method for the fabrication of graphene film on GCE by the electrochemical reduction of electrostatically assembled GO. Initially, 1,6-hexanediamine (HDA) was attached on GCE, and then GO was self-assembled through electrostatic interaction between positively charged amine terminal and the negatively charged groups present in GO followed by the electrochemical reduction of GO. The GO- and ERGO-modified electrodes were characterized by Raman spectroscopy, X-ray diffraction (XRD), attenuated total reflectance Fourier transform infrared spectroscopy (ATR-FT−IR), atomic force microscopy (AFM), and scanning electron microscopy (SEM). Modification of graphene on GCE has several advantages over Au electrode including low cost, wide potential window, relatively inert electrochemistry, and electrocatalytic activity toward a variety of redox reactions.[54] Further, the present strategy of attaching graphene via diamine linker on GCE has several benefits over the reported methods.[32,48−53] Unlike the thiol group, the amine group attached on GCE may not be desorbed at more negative potential. The present modification does not involve any electrochemical pretreatment of GCE.[32,52] The electrocatalytic activity of the present ERGO-modified GCE was examined by taking ascorbic acid (AA), dopamine (DA), and uric acid (UA) as the probes. The ERGO-modified electrode not only enhanced the oxidation currents of AA, DA, and UA but also shifted the oxidation potentials of them to less positive potentials compared to bare GCE. The present modified electrode has low susceptibility to surface fouling and hence used for the simultaneous determination of AA, DA, and UA. The electrochemical response for the oxidation of UA does not change appreciably for several days when it was kept in buffer solution.

EXPERIMENTAL SECTION

Materials. Graphite powder and 1,6-hexanediamine (HDA) were purchased from Alfa Aesar. Potassium permanganate ($KMnO_4$), sodium nitrate ($NaNO_3$), sulfuric acid (H_2SO_4), hydrogen peroxide (H_2O_2), and ascorbic acid (AA) were purchased from Merck, India, and were used as received. Hydrazine hydrate, dopamine (DA), L-histidine (L-His), and uric acid (UA) were purchased from Sigma-Aldrich and were used as received. 0.2 M phosphate buffer solution was prepared using Na_2HPO_4 and NaH_2PO_4. All other chemicals were of analytical grade and were used as received. Double distilled water was used for preparing all solutions. Indium tin oxide (ITO) plates were purchased from Asahi Beer Optical Ltd., Japan.

Instrumentation. The electrochemical measurements and ac electrical impedance spectra were carried out with CHI electrochemical workstation (Model 643B, Austin, TX). Electrochemical measurements were performed in a conventional two-compartment three-electrode cell with GCE as a working electrode, platinum wire as a counter electrode, and NaCl-saturated Ag/AgCl as a reference electrode. Raman spectra were recorded on a Bruker senterra dispersive Raman microscope with laser excitation wavelength of 532 nm. XPS measurements were carried out by using Shimadzu Axis 165 high performance multitechnique analysis using an Al Kα source with pass energy of 80 eV, where the pressure in the analysis chamber was lower than 1×10^{-8} Torr and the dwell time was 458 ms. The binding energies for identical samples were reproducible within ±0.10 eV. X-ray diffraction analysis was carried out with a Rigaku X-ray diffraction unit using Ni-filtered Cu Kα (λ = 1.5406 Å) radiation. The tapping mode AFM images were recorded using a multimode scanning probe microscope (NTMDT, NTEGRA prima, Russia). Scanning electron microscope (SEM) measurements were carried at VEGA3 TESCAN. The FT-IR measurements were carried out in JASCO FT-IR 460 plus model. Attenuated total reflectance infrared (ATR-FT-IR) measurements were carried out using JASCO FT-IR 460 plus model equipped with horizontal ZnSe crystal (Pike Technologies). All the electrochemical experiments were carried out under a nitrogen atmosphere at room temperature.

Synthesis of GO. GO was synthesized using the Hummer's method with a slight modification.[55] Concentrated H_2SO_4 (12 mL) was added to flake graphite (0.5 g) and $NaNO_3$ (0.25 g), and the mixture was cooled to 0 °C. $KMnO_4$ was added slowly into the mixture, and the temperature was maintained at 20 °C. The reaction mixture was warmed to 35 °C and stirred for 30 min. Then, 23 mL of water was added, which produce an exotherm to 98 °C, and the temperature was maintained for 15 min by external heating. The reaction was terminated by the large addition of water (72 mL) and 0.5 mL of 30% H_2O_2. Finally, the reaction mixture was cooled, washed with 0.1 M HCl and water to remove the metal ions, and then dried.

Synthesis of Chemically Reduced GO from GO. Chemical reduction of GO was carried out by the reported procedure using hydrazine hydrate as a reducing agent.[27] Briefly, 0.1 g of GO was mixed with 100 mL of water and sonicated for 45 min to get the clear solution of GO. The pH of

dx.doi.org/10.1021/jp400066z | J. Phys. Chem. C 2013, 117, 4326−4335

Scheme 1. Schematic Illustration for the Modification of ERGO on GCE

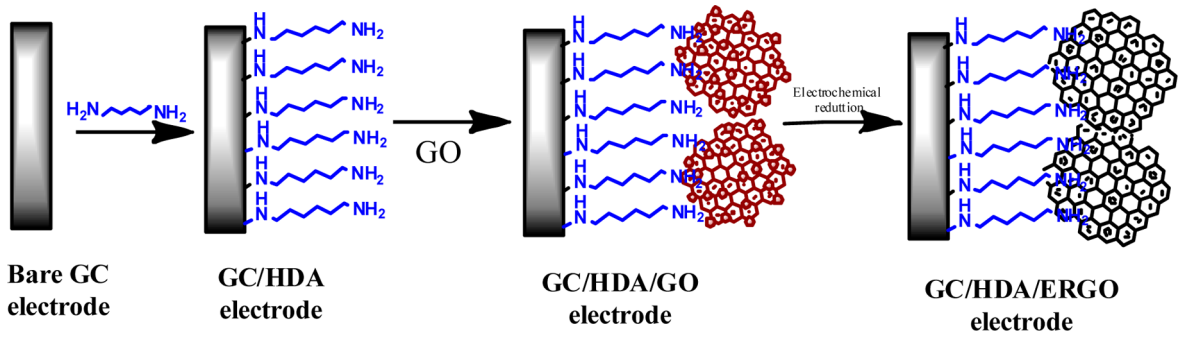

the solution was adjusted to 9 by the addition of saturated sodium carbonate solution. Then, 1 mL of hydrazine hydrate was added, and the reaction mixture was refluxed for 24 h. The precipitated product was filtered and dried.

Fabrication of GCE with GO. The well-cleaned GCE was immersed into 1 mM solution of 1,6-hexanediamine (HDA) for 8 h. The resulting HDA modified electrode was termed as GC/HDA electrode. It was rinsed with water and then immersed into exfoliated GO solution (1 mg/mL) for 12 h. The exfoliation of GO was achieved by the sonication of GO for 45 min. The GO was self-assembled on GC/HDA-modified electrode via electrostatic interaction between positively charged amine groups and negatively charged carboxyl groups present in the GO solution. This electrode is termed as GC/HDA/GO electrode. Then, the GO-modified electrode was electrochemically reduced in PB solution (pH 7) for the fabrication of graphene on GCE. This electrode is termed as GC/HDA/ERGO electrode. Scheme 1 illustrates the schematic representation for the modification of GCE with ERGO.

RESULTS AND DISCUSSION

Electrochemical Reduction of Self-Assembled GO on GCE. For the fabrication of GO on GCE, 1,6-hexanediamine (HDA) was first introduced on GCE by the self-assembly method. The mechanism of amine attachment on GCE follows the Michael's nucleophilic addition of amine group on the olefinic bond present in GCE.[56,57] The pH of the synthesized colloidal suspension of exfoliated GO is 2.5. Since the amine groups of HDA were protonated at pH 2.5, the negatively charged graphene sheets were electrostatically assembled on GC/HDA electrode. The GO attached GC/HDA electrode was electrochemically cycled between 0 and −1.4 V for 15 cycles for the reduction of oxygen functional groups such as epoxide, carboxyl, and hydroxyl present on the surface of GO and to retain the lattice of graphene (Figure 1). In the first cycle, a cathodic peak at −1.15 V appeared which might be due to the reduction oxygen functional groups present on the surface of GO. In the second cycle, the reduction peak current was decreased, and it completely vanished in the subsequent cycles. This indicates the complete reduction of oxygen functional groups present on the surface of GO. The oxygen functional groups introduced during the chemical oxidation were electrochemically reduced, and hence the sp^2 backbone of graphene sheets was regenerated. To find the possible mechanism for the electrochemical reduction of GO, we have recorded CVs at different pH. The GO reduction potential was shifted to more negative potential when the pH was increased, indicating the involvement of proton in the electroreduction process. This is in accordance with the recent paper reported by

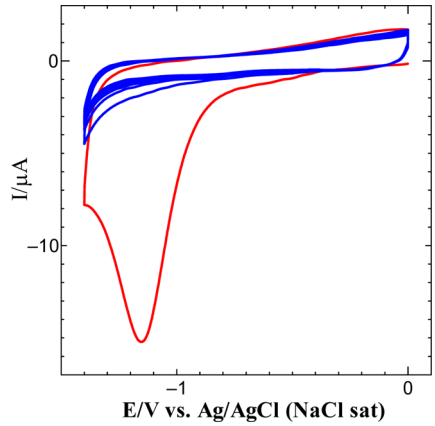

Figure 1. Electrochemical reduction of electrostatically assembled GO on GC/HDA electrode (15 cycles) in 0.2 M PB solution (pH 7.2) at a scan rate of 100 mV s^{-1}.

Dong et al.[36] We have proposed the following mechanism for the electrochemical reduction of GO:

$$GO + aH^+ + be^- \rightarrow \text{graphene} + cH_2O$$

For ATR-FT-IR, Raman, XPS, XRD, AFM, and SEM measurements, we have used ITO as a substrate. We have maintained identical experimental conditions for the deposition of GO and ERGO on ITO substrate.

Characterization by ATR-FT-IR Spectroscopy. ATR-FT-IR spectroscopy was used to confirm the attachment of GO and the removal of oxygen functional groups after electrochemical reduction. Figure S1 shows the FT-IR spectra for powder GO and chemically reduced GO (CRGO) (curves a and b) and ATR-FT-IR spectra obtained for ITO/HDA/GO and ITO/HDA/ERGO substrates (curves c and d). The spectrum of powder GO shows the bands at 1715 (ν(C═O)), 1315 (ν(O−H)), 1620 (ν(C═C)), and a broad band at 3365 cm^{-1} (ν(−OH)) due to intercalated water molecules present on GO. The ATR-FT-IR spectrum of ITO/HDA/GO substrate shows peaks at 1718 (ν(C═O)), 1320 (ν(O−H)), 1618 (ν(C═C)), and 3419 cm^{-1} which is similar to that of powder GO, confirming the successful attachment of GO via HDA linker. After the chemical reduction of powder GO, the peaks at 1715, 1015, and 1315 cm^{-1} were disappeared, suggesting the removal of oxygen functional groups. In the ATR-FT-IR spectrum of ITO/HDA/ERGO substrate, the peaks at 1718 (ν(C═O)) and 1320 cm^{-1} (ν(O−H)) were disappeared, which closely matches with the spectrum of CRGO, indicating that the oxygen functionalities can also be successfully removed by electrochemical reduction. The peak assignments are

dx.doi.org/10.1021/jp400066z | J. Phys. Chem. C 2013, 117, 4326−4335

summarized in Table S1. The above results confirm the attachment of GO on ITO substrate and the removal of oxygen functional groups after the electrochemical reduction.

Characterization by Raman Spectroscopy. Raman spectroscopy is a widely used tool to characterize carbon products due to increase in Raman intensities by the conjugated and double carbon−carbon bonds.[58−60] G and D bands of carbon products are assigned to the E_{2g} phonon of sp^2 carbon atom and the breathing mode of κ-point phonons of A_{1g} symmetry, respectively.[61] Figure 2 shows the Raman spectra

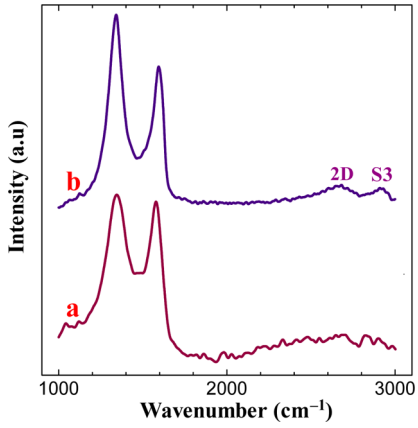

Figure 2. Raman spectra obtained for (a) ITO/HDA/GO and (b) ITO/HDA/ERGO substrates.

of ITO/HDA/GO and ITO/HDA/ERGO substrates. The Raman spectrum of GO-modified ITO substrate shows D and G bands at 1339 and 1582 cm^{-1}, respectively, similar to the peaks observed for powder GO prepared by the chemical oxidation of pristine graphite (curve a: Figure S2). After electrochemical reduction of ITO/HDA/GO substrate, the Raman spectrum displayed an increase in the intensity of D band compared to that of G band (curve c). The increase in the intensity of D band is very similar to CRGO (curve a: Figure S2). The ratio of the intensities of the D and G bands (I_D/I_G) of carbon products is usually used to demonstrate the extent of chemical modification or defects which arise from vacancies, distortion, and edges.[27,61] The larger I_D/I_G value is an indication of greater sp^2 character.[61] As shown in Figure 2, the increase in the intensity ratio (I_D/I_G = 1.39) for ITO/HDA/ERGO substrate compared to ITO/HDA/GO substrate (I_D/I_G = 1.02) suggests a decrease in the average size of the sp^2 domain upon the electrochemical reduction of the exfoliated GO. It shows that the reduction process alters the structure of GO with structural defects. The appearance of 2D (2665 cm^{-1}) and S3 (2911 cm^{-1}) bands at the ITO/HDA/ERGO substrate indicates the better graphitization by electrochemical reduction compared to chemical reduction.[62] The above results suggested the successful attachment of GO on ITO plate through HDA linker, and its electrochemical reduction retained the sp^2-hybridized lattice of graphene. The peak assignments and the I_D/I_G values are summarized in Table S2. Based on D/G intensity ratio obtained in Raman spectra, the average crystalline size was calculated using eq 1.[63]

$$L_a = (2.4 \times 10^{-10})\lambda_{laser}{}^4 \left(\frac{I_D}{I_G}\right)^{-1} \quad (1)$$

where L_a is the average crystalline size and λ is the laser wavelength in nm. The calculated average crystalline sizes of powder GO and CRGO and ITO/HDA/GO and ITO/HDA/ERGO substrates are 21.57, 15.89, 20.72, and 15.20 nm, respectively, indicating the decrease in average crystalline size of GO by both chemical and electrochemical reduction.

Characterization by XPS. Further, XPS was used to confirm the attachment of GO and its electrochemical reduction. Figure 3A shows the XPS survey spectrum of

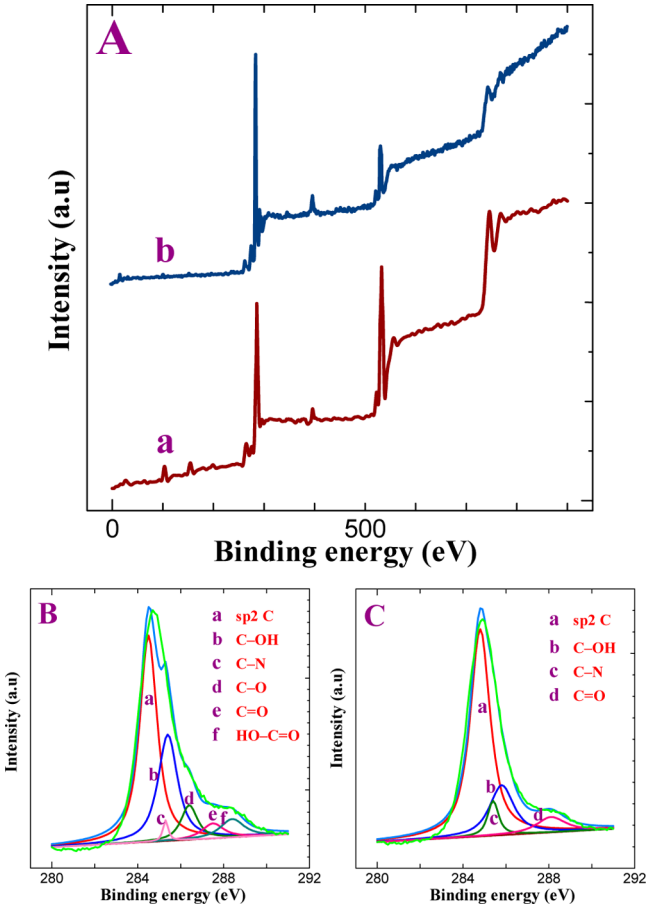

Figure 3. (A) XPS survey spectra obtained for (a) ITO/HDA/GO and (b) ITO/HDA/ERGO plates. XPS C 1s spectra obtained for (B) ITO/HDA/GO and (C) ITO/HDA/ERGO substrates.

ITO/HDA/GO and ITO/HDA/ERGO substrates. The ITO/HDA/GO substrate shows an asymmetric peak at 284.4 eV along with peaks at higher binding energy side. The peak at 284.4 eV corresponds to the C 1s peak of sp^2 carbon (curve a). The peak at 531 eV corresponds to the O 1s spectrum of various oxygen functional groups. The intensity ratio of C/O peaks was calculated as 1.18. After the electrochemical reduction of GO attached on ITO substrate, the XPS spectrum shows C 1s and O 1s peaks at 284.4 and 531 eV, respectively, with a variation in the C/O intensity ratio (curve b). The appearance of small peak at 399 eV for both ITO/HDA/GO and ITO/HDA/ERGO substrates might be due to the amine functionality of HDA linker. The C/O intensity ratio was increased from 1.18 to 4.32 for GO-modified ITO substrate after electrochemical reduction. This is due to the removal of oxygen functional groups from the surface of GO. The above results are consistent with those observed for both powder GO

dx.doi.org/10.1021/jp400066z | J. Phys. Chem. C 2013, 117, 4326−4335

and CRGO (Figure S3A). The attachment of GO on the ITO substrate and its electrochemical reduction were also confirmed by fitting C 1s spectra of ITO/HDA/GO and ITO/HDA/ERGO substrates using Gaussian functions after background correction. Figures 3B and 3C show the C 1s spectrum of ITO/HDA/GO and ITO/HDA/ERGO substrates. The C 1s spectrum of ITO/HDA/GO substrate shows six peaks at 284.5, 285.3, 285.4, 286.4, 287.6, and 288.4 eV, corresponding to sp^2 carbon, C−N bond, C−OH bond, C−O bond, C═O bond, and HO−C═O bond, respectively.[64,65] The binding energy of C−O−C was similar to the binding energy of the C−OH bond, and hence it was not observed in the fitting. On the other hand, the C 1s spectrum of ITO/HDA/ERGO substrate shows four peaks at 284.5, 285.3, 285.6, and 288.1 eV, corresponding to the sp^2 carbon, C−N bond, C−OH bond, and C═O bond, respectively. The appearance of the C−N peak is due to the presence of the C−N bond in HDA linker. In Figure 3C, the intensity of the C═O band was increased at the ITO/HDA/ERGO substrate, which may be due to merging of intensity of C═O bond with $\pi-\pi^*$ shake-up peak of C_2.[29] The intensity of sp^2 C was high, and the intensity of oxygen-containing functional groups was less at the ITO/HDA/ERGO substrate compared to the ITO/HDA/GO substrate, indicating the regeneration of aromatic lattice after the electrochemical reduction of GO. The C 1s spectra of ITO/HDA/GO and ITO/HDA/ERGO plates fitted with Gaussian function were similar to powder GO and CRGO (Figures S3B and S3C), respectively, confirming the attachment of GO through HDA linker, and its electrochemical reduction removes the oxygen functionalities on the electrode surface. The C/O ratio and the peak assignments are summarized in Table S2.

Characterization by XRD. The surface chemistry of GO before and after its electrochemical reduction was studied by XRD. Figure 4 shows the XRD patterns of pristine graphite,

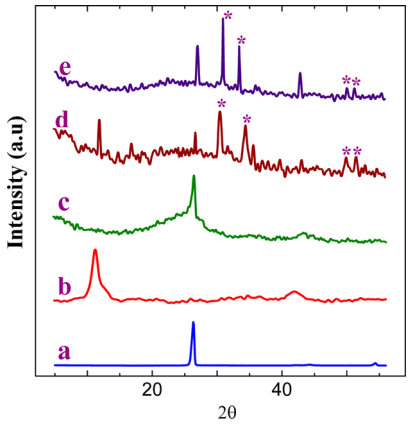

Figure 4. X-ray diffraction pattern for (a) pristine graphite, (b) GO powder, (c) CRGO, and (d) ITO/HDA/GO and (e) ITO/HDA/ERGO substrates.

GO, CRGO, ITO/HDA/GO, and ITO/HDA/ERGO substrates. Pristine graphite shows the diffraction peak at 26.5° (002), 44.3° (101), and 54.2° (004) (curve a), whereas the diffraction peak of GO appears at 11.07° (002), which is the characteristic peak of GO (curve b).[66] The disappearance of the peak at 26.5° after the oxidation process suggests the formation of GO during the oxidation process. After the reduction of GO using hydrazine, the peak at 11.07° (002) of GO disappeared and the peak at 26.46° (002) was restored (curve c). This indicates the removal of oxygen functional groups on the surface of GO and restored the crystal structure of graphene. On the other hand, ITO/HDA/GO substrate shows the characteristic peak of GO at 11.26° similar to the peak obtained for powder GO (curve d), confirming the attachment of GO on ITO substrate. After the electrochemical reduction of self-assembled GO, the peak at 11.26° completely disappeared. Thus, the crystalline nature of graphene was regenerated by the removal of oxygen functional groups during electrochemical reduction which is evidenced from the appearance of peak at 26.39° (curve d), similar to the XRD pattern of CRGO (curve b). The peaks obtained at 30.57°, 35.32°, 49.58°, and 50.85° for ITO/HDA/GO and ITO/HDA/ERGO substrates are the characteristic peaks of ITO (JCPDS File No. 89-4599). It is concluded from the XRD pattern that the GO was self-assembled on ITO substrate, and its electrochemical reduction results in the regeneration of graphite lattice on the surface of ITO.

Morphological Characterization by AFM and SEM. The topography of ITO/HDA/GO and ITO/HDA/ERGO substrates was characterized by AFM and SEM. Figure 5 shows the tapping mode AFM images of ITO/HDA/GO and ITO/HDA/ERGO substrates. The GO-modified film shows homogeneously ordered structure (Figure 5A), whereas ERGO film shows more aggregated rough surface (Figure 5B). This is ascribed to an increase in van der Waals attraction between adjacent layers due to the removal of oxygen functional groups during electrochemical reduction. The increased π-interaction and hydrophobicity make the ERGO film as submicro islands rather than homogeneous layer after electrochemical reduction of GO. Figure S4 shows the SEM images obtained for ITO/HDA/GO and ITO/HDA/ERGO substrates. The GO film showed folded sheets, whereas ERGO film showed more disordered and aggregated structures. The aggregated structure of ERGO confirms the efficient electrochemical reduction of GO.

Characterization by Electrical Impedance Spectroscopy. Graphene sheets modified GCE can also relay the electron transfer between the electroactive species in solution and the underlying electrode. In order to investigate the conducting nature of GC/HDA/GO and GC/HDA/ERGO electrodes, electrical impedance spectroscopy (EIS) was used. Figure 6 shows the Nyquist and Bode plots obtained for bare GC, GC/HDA, GC/HDA/GO, and GC/HDA/ERGO electrodes in 1 mM $[Ru(NH_3)_6]^{3+}$ containing 0.2 M PB solution (pH 3). A Randles circuit model ($R_s[CPE-R_p]$) was used to fit the impedance spectral data. The charge transfer resistance (R_{CT}) can be calculated from the semicircle obtained in the Nyquist plot. An increase in R_{CT} value is observed after the attachment of HDA on GCE due to the electrostatic repulsion between positively charged amine terminal of GC/HDA electrode and $[Ru(NH_3)_6]^{3+/2+}$ redox couple. The insulating nature of GO increases the R_{CT} of GC/HDA/GO electrode compared to bare GC and GC/HDA electrodes. After the electrochemical reduction, the R_{CT} value was decreased compared to that of GC/HDA and GC/HDA/GO electrodes due to regeneration of sp^2 backbone of graphene sheets by the removal of oxygen functional groups which enhances the electrical conductivity. From the Bode phase angle plot (Figure 6B), the maximum phase shift between current and the voltage (−65.92°) was observed at GC/HDA/GO electrode compared to bare GC, GC/HDA, and GC/HDA/ERGO electrodes due to the insulating nature of GO. Though the GO film shows insulating

dx.doi.org/10.1021/jp400066z | J. Phys. Chem. C 2013, 117, 4326−4335

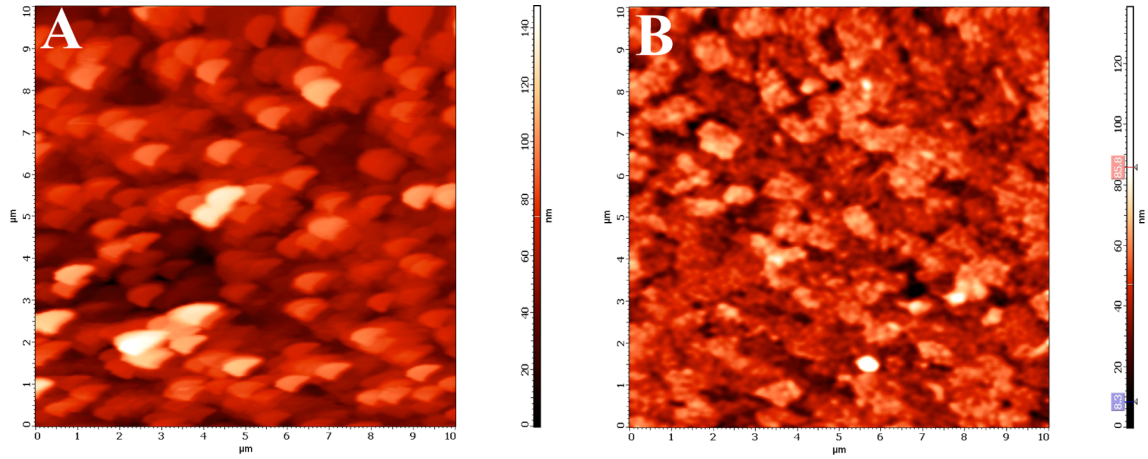

Figure 5. Tapping mode AFM images obtained for (A) ITO/HDA/GO and (B) ITO/HDA/ERGO substrates.

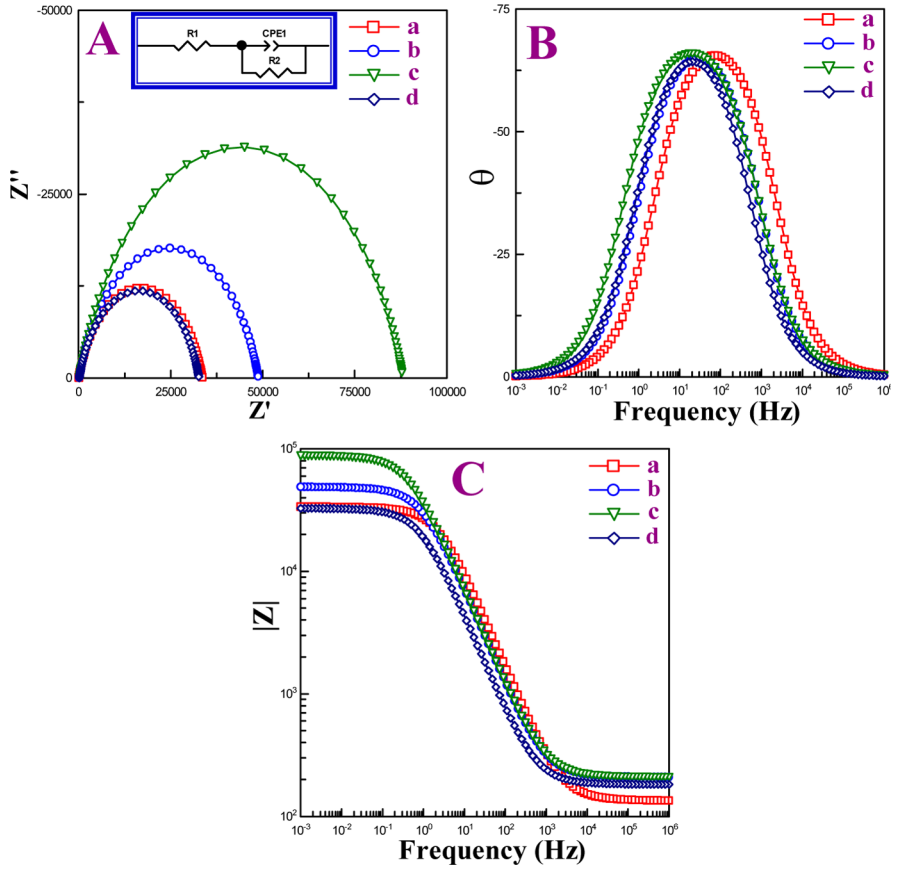

Figure 6. (A) Nyquist plots, (B) Bode-phase angle plots, and (C) Bode amplitude plots for (a) bare GC, (b) GC/HDA, (c) GC/HDA/GO, and (d) GC/HDA/ERGO electrodes in 1 mM $[Ru(NH_3)_6]Cl_3$ containing 0.2 M PB solution (pH 3) at scanning frequencies from 0.01 to 100 000 Hz. Inset: equivalent electrical circuit used for fitting the impedance spectra.

nature, the phase shift value does not reach close to the phase shift value of an ideal capacitor due to the less compact layer of HDA on GCE. After the electrochemical reduction of GO, the phase angle was decreased (−64.25°) compared to that of GC/HDA/GO electrode, indicating the facile electron transfer reaction at GC/HDA/ERGO electrode. In Bode amplitude plot (Figure 6C), the |Z| value in the frequency range from 10^6 to 10^4 was constant, indicating that the solution resistance (R_s) is the same for all the electrodes. Because of the increasing capacitive role, the |Z| value was increased in the frequency region from 10^4 to 10^0 and becomes constant in the frequency region from 10^0 to 10^{-3}, indicating the total resistance of the system ($R_s + R_{CT}$). Since the R_s is same for all the electrodes, it is evident from Figure 6C that the R_{CT} value was increased for the GC/HDA/GO electrode compared to bare and GC/HDA electrodes. After the electrochemical reduction, the R_{CT} was decreased, indicating the conducting nature of ERGO film. The heterogeneous electron transfer rate constant (k_{et}) was calculated using eq 2

$$k_{et} = \frac{RT}{n^2F^2AR_{CT}c^0} \quad (2)$$

dx.doi.org/10.1021/jp400066z | J. Phys. Chem. C 2013, 117, 4326−4335

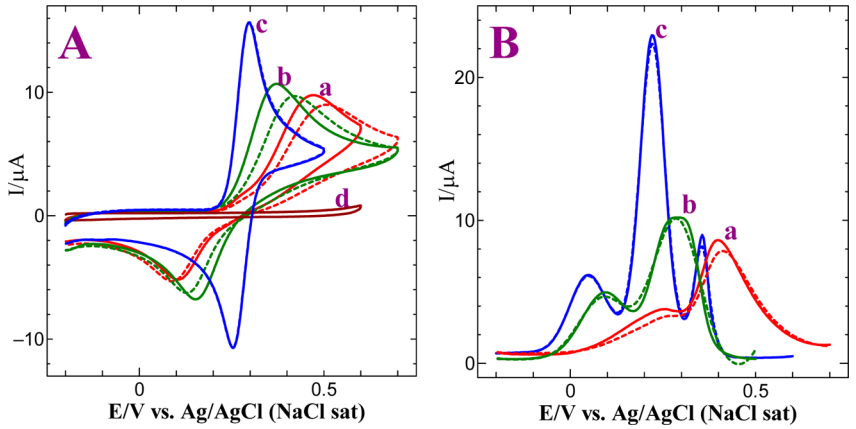

Figure 7. (A) CVs obtained for the oxidation of 0.5 mM of DA at (a) bare GC, (b) GC/HDA/GO, and (c) GC/HDA/ERGO electrodes in 0.2 M PB solution (pH 5.5) at a scan rate of 50 mV s^{-1}. Solid line: first cycle; dotted line: eighth cycle. (B) DPVs obtained for the oxidations of each 0.5 mM of AA, DA, and UA at (a) bare GCE, (b) GC/HDA/GO, and (c) GC/HDA/ERGO electrodes in 0.2 M PB solution. Solid line: first cycle; dotted line: eighth cycle.

where R is the gas constant, T is the temperature (K), F is the Faraday constant, A is the area of the electrode, c^0 is the concentration of the redox probe, and n is the number electrons transferred per molecule of redox probe (n = 1 for $[Ru(NH_3)_6]^{3+/2+}$ probe). The impedance spectral data are tabulated in Table S3. The k_{et} values are 4.29×10^{-5} and 1.16×10^{-4} cm s^{-1} for GC/HDA/GO and GC/HDA/ERGO electrodes. The obtained higher value indicates that the electron transfer reaction was facile at ERGO films-modified electrode compared to the GO-modified electrode.

Electrocatalytic Activity of ERGO-Modified Electrode toward Ascorbic Acid, Dopamine, and Uric Acid. It is well-known that graphene sheets show good electrical conductivity, and therefore the electrodes modified with them can be used in electrocatalytic applications.[13,14] In the present study, the electrocatalytic property of ERGO film was examined by taking AA, DA, and UA as the probes. Figure S5A shows the CVs obtained for 0.5 mM AA at bare GC, GC/HDA/GO, and GC/HDA/ERGO electrodes in 0.2 M PB solution (pH 5.5). Bare GCE oxidizes AA at 0.32 V (curve a: solid line), and the oxidation current decreases along with the potential shift toward more positive potential for further potential cycles (curve a: dotted line). Though the oxidation peak current of AA was enhanced along with the less positive potential shift at GC/HDA/GO electrode compared to bare GCE, the oxidation peak was not stable for further potential cycles (curve b). In the case of the GC/HDA/ERGO electrode, the oxidation peak was shifted to less positive potential with enhanced peak current compared to bare GC and GC/HDA/GO electrodes (curve c: solid line). Moreover, the oxidation peak potential and current remain unchanged even after eight cycles at GC/HDA/ERGO electrode (curve c: dotted line). Figure 7A shows the CVs obtained for 0.5 mM DA at bare GC, GC/HDA/GO, and GC/HDA/ERGO electrodes in 0.2 M PB solution. The oxidation of DA was observed at 0.47 V at bare GCE (curve a: solid line), and after eight cycles, decrease in peak current and shifting of oxidation potential to more positive potential were observed due to surface fouling effect caused by the oxidation products of DA (curve a: dotted line). At GC/HDA/GO electrode, DA oxidation was observed at 0.37 V (curve b: solid line), and the oxidation peak was not stable after eight cycles (curve b: dotted line). On the other hand, the oxidation of DA was observed at 0.29 V with enhanced oxidation current at GC/HDA/ERGO electrode compared to bare GC and GC/HDA/GO electrodes (curve c: solid line). Moreover, the oxidation peak of DA was stable at GC/HDA/ERGO electrode after eight cycles (curve c: dotted line). The enhanced oxidation current, shifting of oxidation potential toward less positive potential, and decreasing the peak separation of DA compared to bare GC and GC/HDA/GO electrodes might be due to the $\pi-\pi$ interaction between the aromatic moieties of DA and ERGO film besides the facile electron transfer reaction through ERGO film from the underlying electrode. Figure S5B shows the oxidation of UA at bare GC, GC/HDA/GO, and GC/HDA/ERGO electrodes. Similar to AA and DA oxidation, the oxidation peak current of UA was greatly enhanced with less positive potential shift at GC/HDA/ERGO electrode compared to bare GC and GC/HDA/GO electrodes. In the subsequent potential cycles, the oxidation peak of UA was stable at GC/HDA/ERGO electrode (curve c), whereas slight shift in the potential and decrease in the oxidation current were observed at bare GC and GC/HDA/GO electrodes (curves a and b). Further, the effect of scan rate for the oxidations of DA, AA, and UA was studied at the ERGO-modified electrode (Figure S6). While increasing the scan rate from 25 to 200 mV, the oxidation peak current was increased linearly. The plots of oxidation peak current versus the square root of scan rate were linear with correlation coefficients of 0.9992, 0.9996, and 0.9993 for DA, AA, and UA, respectively (inset: Figure S6), indicating that the oxidations of DA, AA, and UA were controlled by diffusion at GC/HDA/ERGO electrode. Figure 7B shows the differential pulse voltammograms (DPVs) obtained for the oxidations of each 0.5 mM AA, DA, and UA in a mixture at bare, GC/HDA/GO, and GC/HDA/ERGO electrodes. Bare GC and GC/HDA/GO electrodes did not separate the oxidation peaks of DA and UA (curves a and b). This shows that bare GC and GC/HDA/GO electrodes were not suitable for the determination of AA, DA, and UA in a mixture. In the case of GC/HDA/ERGO electrode, the oxidation peaks of AA, DA, and UA were well separated and were stable for further potential cycles. The effective $\pi-\pi$ interaction between the aromatic moieties of DA and ERGO shifted the oxidation of DA toward less positive potential, and hence the oxidation peaks of DA and UA were well separated at the GC/HDA/ERGO electrode. This result suggested that the GC/HDA/ERGO electrode was highly suitable for the

dx.doi.org/10.1021/jp400066z | J. Phys. Chem. C 2013, 117, 4326−4335

simultaneous determination of the AA, DA, and UA in a mixture. Figure S7 shows the DPVs obtained for the increment of 20 μM AA, 5 μM DA, and 10 μM UA in a mixture at GC/HDA/ERGO electrode in 0.2 M PB solution. A well-defined oxidation peaks were observed for 20 μM AA, 5 μM DA, and 10 μM UA at 0.06, 0.22, and 0.34 V, respectively. For each increment of AA, DA, and UA, the peak currents of the respective analytes were increased linearly. To examine the sensitivity of GC/HDA/ERGO electrode, the amperometric method was used. Figure S8 shows the amperometric $i-t$ curve for DA at the GC/HDA/ERGO electrode in a homogeneously stirred 0.2 M PBS by applying constant potential of +0.35 V. The GC/HDA/ERGO electrode shows the initial current response due to 50 nM DA, and further additions of 50 nM DA in each step with a sample interval of 50 s increase the current response (Figure S7A). The dependence of current response with respect to concentration was linear from 50 to 600 nM for DA with correlation coefficient of 0.9992 (inset: Figure S8A). Further, the amperometric current response was linearly increased with increasing concentration in the dynamic range of 50×10^{-9}–40×10^{-5} M for DA (Figure S8B), and the detection limit was found to be 19×10^{-9} M (S/N = 3).

To demonstrate the advantage of the present alkyldiamine linker for the attachment of graphene, we have examined the oxidation of L-histidine (L-His), which usually oxidizes at more than 1 V at bare GCE. Figure 8 shows the oxidation of L-His at

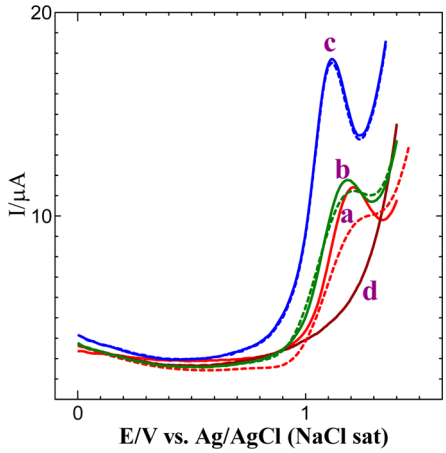

Figure 8. DPVs obtained for the oxidation of 0.5 mM of L-His at (a) bare GC, (b) GC/HDA/GO, and (c) GC/HDA/ERGO electrodes in 0.2 M PB solution (pH 7.2). (d) CVs of GC/HDA/ERGO electrode in 0.2 M PB solution in the absence of L-His. Solid line: first cycle; dotted line: eighth cycle.

bare GC and GC/HDA/ERGO electrodes in 0.2 M PB solution. Bare GCE oxidizes L-His at 1.18 V (curve a: solid line), and after eight cycles, the oxidation potential was shifted to more positive potential and a decrease in peak current was observed (curve a: dotted line). Although the oxidation current was slightly enhanced at GC/HDA/GO electrode (curve b: solid line), the oxidation current was not stable on further potential cycles (curve b: dotted line). On the other hand, GC/HDA/ERGO electrode oxidizes L-His at 1.11 V with enhanced peak current in contrast to bare GCE and the oxidation peak remains unchanged even after eight potential cycles (curve b: dotted line). It is well-known that the Au–S bond will get oxidized at more positive potential.[67,68] Hence, it is not possible to sense the biomolecules oxidizing at more positive potential using thiol-based linkers. In contrary, as demonstrated in Figure 8, the HDA linker used in the present study will be stable at more positive potential, and thus it can be used to study the oxidation of L-His. Hence, the present method of graphene modification can be used to sense the biomolecules in a wide potential range. It has been reported that the oxidation of L-His was not stable at bare electrodes including GCE due to the strong adsorption of the oxidized products on electrode surfaces.[69] As shown in Figure 8, the GC/HDA/ERGO electrode effectively prevented the surface fouling effect caused by the oxidation products of L-His, and hence the oxidation was stable at the present modified electrode. The detailed studies for the determination of L-His using the GC/HDA/ERGO electrode will be published elsewhere.

Stability and Reproducibility of the ERGO-Modified Electrode. In order to investigate the stability of GC/HDA/ERGO electrode, the oxidation of UA was recorded for a week at physiological pH solution. Figure 9 shows the DPVs

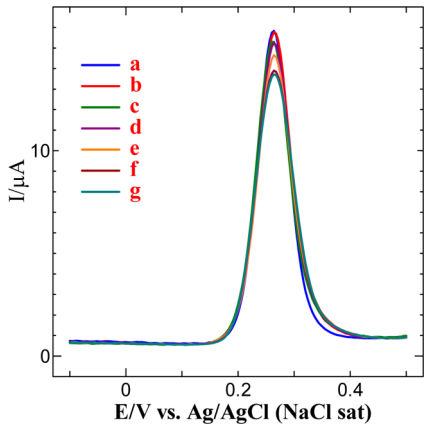

Figure 9. DPVs obtained for the oxidation of 0.5 mM UA at the GC/HDA/ERGO electrode in 0.2 M PB solution at different days: (a) 1, (b) 2, (c) 3, (d) 4, (e) 5, (f) 6, and (g) 7.

obtained for 0.5 mM UA at GC/HDA/ERGO electrode in 0.2 M PB solution (pH 7.2) from the first day to seventh day (curves a–g). The UA oxidation potential remains unchanged from the first day to seventh day. However, the oxidation peak current slightly decreases for the first 5 days, and after that no significant decrease in oxidation peak current was observed for the days 6 and 7 (Figure 9). The fouling percentage was measured based on the difference in oxidation peak currents of UA from first day to seventh day, and it was found to be 9.5%. Further, to check the reproducibility of the results, three different GC electrodes were fabricated with ERGO under similar conditions. Their current response and peak potential toward the oxidation of UA were the same at all three electrodes. The above results showed that the present modified electrode was very much stable and reproducible.

CONCLUSIONS

The present work demonstrated a simple, facile, and reproducible method for the modification of GCE with graphene backbone. The graphene precursor GO was preassembled on GCE through a diamine linker via electrostatic attraction between positively charged amine groups and the negatively charged layers of graphene oxide. The GO attached GC/HDA electrode was electrochemically reduced to remove the oxygen functional groups present on the layers of GO and

dx.doi.org/10.1021/jp400066z | J. Phys. Chem. C 2013, 117, 4326–4335

to retain the aromatic lattice of graphene. The fabricated thin films of GO and ERGO were characterized by ATR-FT-IR spectroscopy, Raman spectroscopy, XRD, AFM, and SEM. The Raman spectrum shows the increase in the intensity ratio of D and G bands after the electrochemical reduction of GO layer, indicating that the graphene backbone was retained by the removal of oxygen-containing functional groups. AFM images confirm the uniform distribution of graphene layers on the electrode surface. Further, the GC/HDA/ERGO electrode shows good electrocatalytic activity toward AA, DA, and UA. Bare GC and GC/HDA/GO electrodes experience the surface fouling effect, whereas the GC/HDA/ERGO electrode shows low susceptibility to surface fouling and therefore successfully used for the simultaneous determination of them. Moreover, the electrochemical response of present modified electrode does not change appreciably for several days, and hence it may be used for the fabrication of stable sensors.

■ ASSOCIATED CONTENT

Supporting Information

ATR-FT-IR spectral characterization of GO- and ERGO-modified ITO plates; Raman spectra of powder GO and CRGO; XPS wide range and C 1s spectra of powder GO and CRGO; SEM images of GO- and ERGO-modified ITO substrates; CV corresponding to the oxidation of AA and UA; effect of scan rate on the oxidation of AA and UA; amperometric determination of DA; oxidation of L-His at ERGO electrode; table for IR spectral data; table for the peak assignments of Raman spectra and XPS; table for impedance spectral data. This material is available free of charge via the Internet at http://pubs.acs.org.

■ AUTHOR INFORMATION

Corresponding Author

*E-mail: abrajohn@yahoo.co.in.

Notes

The authors declare no competing financial interest.

■ ACKNOWLEDGMENTS

M. Amal Raj thanks the Council of Scientific and Industrial Research (CSIR), New Delhi, for the award of Senior Research Fellowship (09/715(0014)/2010-EMR-I).

■ REFERENCES

(1) Neto, A. H. C.; Guinea, F.; Peres, N. M. R.; Novoselov, K. S.; Geim, A. K. *Rev. Mod. Phys.* **2009**, *81*, 109−162.

(2) Rao, C. N. R.; Sood, A. K.; Voggu, R.; Subramanyam, K. S. *J. Phys. Chem. Lett.* **2010**, *1*, 572−580.

(3) Ratinac, K. R.; Yang, W.; Gooding, J. J.; Thordarson, P.; Braet, F. *Electroanalysis* **2011**, *23*, 803−826.

(4) Bunch, J. S.; van der Zande, A. M.; Verbridge, S. S.; Frank, I. W.; Tanenbaum, D. M.; Parpia, J. M.; Craighead, H. G.; McEuen, P. L. *Science* **2007**, *315*, 490−493.

(5) Shi, Y.; Fang, W.; Zhang, K.; Zhang, W.; Li, L. *Small* **2009**, *5*, 2005−2011.

(6) Novoselov, K. S.; Geim, A. K.; Morozov, S. V.; Jiang, D.; Zhang, Y.; Dubonos, S. V.; Grigorieva, I. V.; Firsov, A. A. *Science* **2004**, *306*, 666−669.

(7) Bolotin, K. I.; Sikes, K. J.; Jiang, Z.; Klima, M.; Fudenberg, G.; Hone, J.; Kim, P.; Stormer, H. L. *Solid State Commun.* **2008**, *146*, 351−355.

(8) Kampouris, D. K.; Banks, C. E. *Chem. Commun.* **2010**, *46*, 8986−8988.

(9) Son, Y.; Cohen, M. L.; Louie, S. G. *Nature* **2006**, *444*, 347−349.

(10) Avouris, P.; Chen, Z.; Perebenios, V. *Nat. Nanotechnol.* **2007**, *2*, 605−615.

(11) Stoller, M. D.; Park, S.; Zhu, Y.; An, J.; Rouff, R. S. *Nano Lett.* **2008**, *8*, 3498−3502.

(12) Takamura, T.; Endo, K.; Fu, L.; Wu, Y.; Lee, K. J.; Matsumoto, T. *Electrochim. Acta* **2007**, *53*, 1055−1061.

(13) Shao, Y.; Wang, J.; Wu, H.; Liu, J.; Aksay, I. A.; Lin, Y. *Electroanalysis* **2010**, *22*, 1027−1036.

(14) Alwarappan, S.; Boyapalle, S.; Kumar, A.; Li, C.-Z.; Mohapatra, S. *J. Phys. Chem. C* **2012**, *116*, 6556−6559.

(15) Wang, X.; Zhi, L.; Müllen, K. *Nano Lett.* **2008**, *8*, 323−327.

(16) Liu, C.; Alwarappan, S.; Chen, Z.; Kong, X.; Li, C. Z. *Biosens. Bioelectron.* **2010**, *25*, 1829−1833.

(17) Si, Y.; Samulski, E. T. *Nano Lett.* **2008**, *8*, 1679−1682.

(18) Guo, H.; Wang, X.; Qian, Q.; Wang, F.; Xia, X. *ACS Nano* **2009**, *3*, 2653−2659.

(19) Shen, J.; Hu, Y.; Shi, M.; Lu, X.; Qin, C.; Li, C.; Ye, M. *Chem. Mater.* **2009**, *21*, 3514−3520.

(20) Park, S.; Dikin, D. A.; Nguyen, S. T.; Ruoff, R. S. *J. Phys. Chem. C* **2009**, *113*, 15801−15804.

(21) Schniepp, H. C.; Li, J. L.; McAllister, M. J.; Sai, H.; Herrera-Alonso, M.; Adamson, D. H.; Prudhomme, R. K.; Saville, D. A.; Aksay, I. A. *J. Phys. Chem. B* **2006**, *110*, 8535−8539.

(22) Lotya, M.; Hernandez, Y.; King, P. J.; Smith, R. J.; Nicolosi, V.; Karlsson, L. S.; Blighe, F. M.; De, S.; Wang, Z.; McGovern, I. T.; Duesberg, G. S.; Coleman, J. N. *J. Am. Chem. Soc.* **2009**, *131*, 3611−3620.

(23) Li, D.; Mueller, M. B.; Gilje, S.; Kaner, R. B.; Wallace, G. G. *Nat. Nanotechnol.* **2009**, *3*, 101−105.

(24) Marcano, D. C.; Kosynkin, D. V.; Berlin, J. M.; Sinitskii, A.; Sun, Z.; Slesarev, A.; Alemany, L. B.; Lu, W.; Tour, J. M. *ACS Nano* **2010**, *4*, 4806−4814.

(25) Staudenmaier, L. *Ber. Dtsch. Chem. Ges.* **1898**, *31*, 1481−1487.

(26) Hummers, W. S.; Offeman, R. E. *J. Am. Chem. Soc.* **1958**, *80*, 1339−1339.

(27) Stankovich, S.; Dikin, D. A.; Piner, R. D.; Kleinhammes, K. A.; Jia, Y.; Wu, Y.; Nguyen, S. B. T.; Ruoff, R. S. *Carbon* **2007**, *45*, 1558−1565.

(28) Wang, G.; Yang, J.; Park, J.; Gou, X.; Wang, B.; Liu, H. *J. Phys. Chem. C* **2008**, *112*, 8192−8195.

(29) Fernandez-Merino, M. J.; Guardia, L.; Paredes, J. I.; Villar-Rodil, S.; Solıs-Fernandez, P.; Martınez-Alonso, A.; Tascon, J. M. D. *J. Phys. Chem. C* **2010**, *114*, 6426−6432.

(30) Fan, X.; Peng, W.; Li, Y.; Li, X.; Wang, S.; Zhang, G.; Zhang, F. *Adv. Mater.* **2008**, *20*, 4490−4493.

(31) Zhou, X.; Zhang, J.; Wu, H.; Yang, H.; Zhang, J.; Guo, S. *J. Phys. Chem. C* **2011**, *115*, 11957−11961.

(32) Wang, Z.; Zhou, X.; Zhang, J.; Boey, F.; Zhang, H. *J. Phys. Chem. C* **2009**, *113*, 14071−14075.

(33) Ping, J.; Wang, Y.; Fan, K.; Wu, J.; Ying, Y. *Biosens. Bioelectron.* **2011**, *28*, 204−209.

(34) Chen, L.; Tang, Y.; Wang, K.; Liu, C.; Luo, S. *Electrochem. Commun.* **2011**, *13*, 133−137.

(35) Fu, C.; Kuang, Y.; Huang, Z.; Wang, X.; Du, N.; Chen, J.; Zhou, H. *Chem. Phys. Lett.* **2010**, *499*, 250−253.

(36) Zhou, M.; Wang, Y.; Zhai, Y.; Zhai, J.; Ren, W.; Wang, F.; Dong, S. *Chem.—Eur. J.* **2009**, *15*, 6116−6120.

(37) Du, M.; Yang, T.; Jiao, K. *J. Mater. Chem.* **2010**, *20*, 9253−9260.

(38) Chen, D.; Tang, L.; Li, J. *Chem. Soc. Rev.* **2010**, *39*, 3157−3180.

(39) Pumera, M. *Chem. Soc. Rev.* **2010**, *39*, 4146−4157.

(40) Brownson, D. A. C.; Banks, C. E. *Analyst* **2010**, *135*, 2768−2778.

(41) Wang, Z.; Shoji, M.; Ogata, H. *Analyst* **2011**, *136*, 4903−4905.

(42) Keeley, G. P.; O'Neill, A.; Holzinger, M.; Cosnier, S.; Coleman, J. N.; Duesberg, G. S. *Phys. Chem. Chem. Phys.* **2011**, *13*, 7747−7750.

(43) Gilje, S.; Han, S.; Wang, M.; Wang, K. L.; Kaner, R. B. A. *Nano Lett.* **2007**, *7*, 3394−3398.

(44) Tung, V. C.; Allen, M. J.; Yang, Y.; Kaner, R. B. *Nat. Nanotechnol.* **2008**, *4*, 25−29.

(45) Cote, L. J.; Kim, F.; Huang, J. *J. Am. Chem. Soc.* **2009**, *131*, 1043−1049.
(46) Hu, X. G.; Dong, S. J. *J. Mater. Chem.* **2008**, *18*, 1279−1295.
(47) Ulman, A. *Chem. Rev.* **1996**, *96*, 1533−1554.
(48) Xie, X.; Zhao, K.; Xu, X.; Zhao, W.; Liu, S.; Zhu, Z.; Li, M.; Shi, Z.; Shao, Y. *J. Phys. Chem. C* **2010**, *114*, 14243−14250.
(49) Yang, S.; Xu, B.; Zhang, J.; Huang, X.; Ye, J.; Yu, C. *J. Phys. Chem. C* **2010**, *114*, 4389−4393.
(50) Ramesha, G. K.; Sampath, S. *J. Phys. Chem. C* **2009**, *113*, 7985−7989.
(51) Viinikanoja, A.; Wang, Z.; Kauppila, J.; Kvarnström, C. *Phys. Chem. Chem. Phys.* **2012**, *14*, 14003−14009.
(52) Wang, Z.; Wu, S.; Zhang, J.; Chen, P.; Yang, G.; Zhou, X.; Zhang, Q. *Nanoscale Res. Lett.* **2012**, *7*, 1−7.
(53) Haque, A.; Park, H.; Sung, D.; Jon, S.; Choi, S.; Kim, K. *Anal. Chem.* **2012**, *84*, 1871−1878.
(54) McCreery, R. L. *Chem. Rev.* **2008**, *108*, 2646−2687.
(55) Kovtyukhova, N. I.; Ollivier, P. J.; Martin, B. R.; Mallouk, T. E.; Chizhik, S. A.; Buzaneva, E. V.; Gorchinskiy, A. D. *Chem. Mater.* **1999**, *11*, 771−778.
(56) Gallardo, I.; Pinson, J.; Vila, N. *J. Phys. Chem. B* **2006**, *110*, 19521−19529.
(57) Sivanesan, A.; John, S. A. *Electrochim. Acta* **2009**, *54*, 7458−7463.
(58) Kudin, K. N.; Ozbas, B.; Schniepp, H. C.; Prudhomme, R. K.; Aksay, I. A.; Car, R. *Nano Lett.* **2008**, *8*, 36−41.
(59) Ferrari, A. C.; Meyer, J. C.; Scardaci, V.; Casiraghi, C.; Lazzeri, M.; Mauri, F.; Piscanec, S.; Jiang, D.; Novoselov, K. S.; Roth, S.; Geim, A. K. *Phys. Rev. Lett.* **2006**, *97*, 187401−187404.
(60) Rao, A. M.; Richter, E.; Bandow, S.; Chase, B.; Eklund, P. C.; Williams, K. A.; Fang, S.; Subbaswamy, K. R.; Menon, M.; Thess, A.; Smalley, R. E.; Dresselhaus, G.; Dresselhaus, M. S. *Science* **1997**, *275*, 187−191.
(61) Tuinstra, F.; Koenig, J. L. *J. Chem. Phys.* **1970**, *53*, 1126−1130.
(62) Tung, V. C.; Allen, M. J.; Yang, Y.; Kaner, R. B. *Nat. Nanotechnol.* **2009**, *4*, 25−29.
(63) Pimenta, M. A.; Dresselhaus, G.; Dresselhaus, M. S.; Cancado, L. G.; Jorio, A.; Saito, R. *Phys. Chem. Chem. Phys.* **2007**, *9*, 1276−1291.
(64) Sundberg, K. M.; Smyrl, W. H.; Atanasoska, Lj.; Atanasoski, R. *J. Electrochem. Soc.* **1989**, *136*, 434−439.
(65) Yumitori, S. *J. Mater. Sci.* **2000**, *35*, 139−146.
(66) Jeong, H.; Lee, Y. P.; Lahaye, J. W. E.; Park, M.; An, K. H.; Kim, I. J.; Yang, C.; Park, C. Y.; Rouff, R. S.; Lee, Y. H. *J. Am. Chem. Soc.* **2008**, *130*, 1362−1366.
(67) Batz, V.; Schneeweiss, M. A.; Kramer, D.; Kramer, D.; Hagenstrom, H.; Kolb, D. M.; Mandler, D. *J. Electroanal. Chem.* **2000**, *491*, 55−68.
(68) Widrig, C. A.; Chung, C.; Porter, M. D. *J. Electroanal. Chem.* **1991**, *310*, 335−359.
(69) Nan, C. G.; Ping, W. X.; Ping, D. J.; Qing, C. H. *Talanta* **1999**, *49*, 319−330.